The role of an intense jet in the Tsugaru Strait in the formation of the outflow gyre revealed using high-frequency radar data

H. Kaneko[1], K. Sasaki[1], H. Abe[1,2], S. Watanabe[1], and Y. Sato[1]

[1] Mutsu Institute for Oceanography, Research Institute for Global Change, Japan Agency for Marine-Earth Science and Technology, Mutsu, Japan.

[2] Faculty of Fisheries Sciences, Hokkaido University, Hakodate, Japan.

Corresponding author: Hitoshi Kaneko (h_kaneko@jamstec.go.jp)

Key Points:

- Observational verification of the seasonal flow pattern theory of the Tsugaru Warm Current based on velocity data from high-frequency radar
- Importance of vorticity gap at the front of the jet recognized in addition to the volume transport of the current on the flow pattern change
- Effectiveness of high-frequency radar with diagnostic scheme improves understanding of the role of the strait in coastal flow around Japan

Abstract

The seasonal pattern of the eastward jet through the Tsugaru Strait between 2014 and 2019 was investigated using surface velocity data obtained from high-frequency radar located in the eastern part of the strait. The vorticity-front-model was used to estimate the volume transport of low-vorticity water and the intensity of the vorticity gap at the front using the climatological mean zonal velocity distribution. The flow mode at the outlet was then defined as either the summer/autumn “gyre mode” or winter/spring “coastal mode”. The distribution of the parameters was consistent with the theoretical understanding, showing that in addition to the volume transport, an increase in the vorticity gap can also contribute to the development of the gyre. The results also suggest an impact from the jet in the strait on the coastal flow along the coast of Japan.

Plain Language Summary

The Tsugaru Warm Current forms part of the coastal flow around Japan and shows remarkable seasonal changes in its flow pattern, which are similar to the Kuroshio meandering. The current flows along the coast from winter to spring, but demonstrates large anticyclonic meandering in the offshore direction, known as “gyre mode”, from summer to autumn. The cause of this change in the flow pattern has been thought to be the seasonal change in volume transport. In this study, we used high-resolution temporal and spatial data obtained from a high-frequency radar system, as well as the relationship between coastal waves and offshore jets with fronts, to identify another important factor that affects the seasonal flow pattern of the current, namely, “vorticity”. Our results demonstrate the applicability and effectiveness of the high-frequency radar monitoring, and that it could be successfully used in other coastal regions, including other parts

of the same strait. Moreover, our study indicates that the response of the flow in the strait to volume transport and vorticity will be important to long-term changes in the wider circulation in relation to global warming and decadal-scale changes.

1 Introduction

The Tsugaru Strait is located between the mainland of Japan (Honshu) and Hokkaido (Figure 1a). The Tsugaru Warm Current (TWC; Figure 1a) is a branch of the Tsushima Warm Current, which itself has origins in the Kuroshio southwest of Kyushu island as well as the flow from the Taiwan Strait (Isobe, 1999). The other branch flows north along the coast of Hokkaido as the Soya Warm Current. These currents are closely related and can be considered one system (e.g., Kida et al., 2016). In the Tsugaru Strait, a recent study (Wakita et al., submitted to GRL) reported faster acidification than that in the global ocean. In addition, a far more intense vertical mixing than in the open ocean, and enhancement of vertical nitrate transport above the characteristic topography in the western part of the strait were also observed (Tanaka et al., 2021). These recent studies suggest these characteristic phenomena that occur in the strait could affect a wider region via the TWC.

The mean volume transport of the TWC and its seasonal variations have been estimated as 1.5 ± 0.3 Sv, (=10^6 m^3 s^{-1}; e.g., Onishi and Ohtani, 1997; Nishida et al., 2003). Based on the sea level difference between Fukaura and Hakodate (Figure 1b), Nishida et al. (2003) also reported that the transport increases from spring to summer (maximum in July and August) and decreases from autumn to winter (minimum in February). As another seasonal variation, there is a remarkable change in the outflow pattern of the TWC from the eastern outlet of the strait. This outflow switches from “coastal mode”, which is a nearshore flow along the coast of the Shimokita Peninsula (in winter and spring), to “gyre mode”, which is a large anticyclonic gyre that develops south of Hokkaido (in summer and autumn) (e.g., Conlon, 1982; Figure 1b). It is thought that the increase in volume transport through the strait could initiate the development of the gyre mode (e.g., Kawasaki and Sugimoto, 1988).

In addition to the volume transport, Kubokawa (1991; hereafter K91) raised another important aspect of the difference in the vorticity across the jet based on the reduced gravity model with vorticity-front (Figure S1). Using parameters such as the transport of water with a relatively lower potential vorticity between the front and the boundary (area A in Figure S1), the vorticity gap at the front, and the total volume transport at the outflow, K91 revealed that an enhancement of the vorticity gap relative to the total volume transport is important for the transition from "coastal" to "gyre" mode, in addition to an exceeding of the volume transport of the lower potential vorticity fluid at the outlet of the strait relative to that at the far downstream region. Although Nof and Pichevin (1999) proposed that the Tsugaru and the Alboran gyres could develop regardless of the initial vorticity, and they also commented on the importance of on-site estimation of vorticity in the currents as a subject for future investigation.

However, because of the lack of temporal and spatial observations from vessels and moorings, the importance of the vorticity associated with the jet remains to be fully clarified. This lack of observational data arises because it is difficult to estimate the mean geostrophic field from time-limited shipboard current measurements, such as those made using acoustic Doppler current profilers, because of the strong tidal current in the strait (Isoda and Baba, 1998; Onishi et al., 2004; Luu et al., 2011; Ohta et al., 2014; Yamaguchi et al., 2020; Matsuura and Isoda, 2020). The use of multiple moorings across the jet is also difficult due to the intense velocity and frequent ship traffic through the strait. Moreover, although satellite observations can provide gridded time series data covering a long period, the spatial resolution with respect to velocity is too coarse for vorticity analysis.

Therefore, in this study, we used high-frequency radar (HFR) for surface current monitoring in the eastern part of the strait (Figure 1c). This system can provide suitably high-

93 resolution spatial data, and also long-term and homogeneously (equally spaced in time)
94 continuous data that allowed us to estimate the background quasi-geostrophic current distribution
95 for the vorticity analysis. Using the data obtained by the HFR system developed by the Mutsu
96 Institute for Oceanography (MIO), Japan Agency for Marine-Earth Science and Technology
97 (JAMSTEC), we confirmed the effect of the vorticity gap at the jet axis based on the diagram
98 proposed by K91. Our results, which are in good agreement with the theory of K91, will be
99 presented below, after a brief explanation of our data analysis methods and the theory described
100 in K91. Moreover, the role of the eastern part of the strait will be discussed from the point of
101 view of the island circulation along the coast, which might be a contributor to the long-term
102 variations and/or rapid shifts in environmental conditions.

103

104 **2 Materials and Methods**

105 Surface velocity data for the eastern Tsugaru Strait were obtained from the MIO ocean
106 radar data site (MORSETS; https://www.godac.jamstec.go.jp/morsets/e/top/). The monitoring
107 system comprises three high-frequency radars (SeaSonde, 13.9 MHz, CODAR Ocean Sensors)
108 located in the Tsugaru Strait: two on the Shimokita Peninsula and the other on Hokkaido (Figure
109 1c). The system yields velocity distributions with a horizontal resolution of approximately 3 km
110 every 30 minutes, and the same system has also been used to monitor the Tsushima Warm
111 Current (e.g., Yoshikawa et al., 2006). We used data covering the period between March 2014,
112 when observations began, and December 2019. Data were collected from within the region
113 bounded by 140.93–141.98°E and 41.38–42.05°N (Figure 1c).

To investigate seasonal changes in the mean velocity field, we estimated the climatological mean of zonal velocity, U, with respect to a series of 5-km zonal bands, which were set from 140.92°E to 142.04°E with a half-overlap (Figure 1c). Within this zone, the climatological mean was estimated each day from January 1st to December 31st over the period 2014–2019, using a width of 10 days. Outliers were excluded if they had a value that fell outside of three standard deviations from the mean. Examples of the seasonal variation of U are shown in Figure 2a and b. The axis of the jet was defined as the latitude of the U-maximum (extremum). In addition, the meridional distribution of U was used to estimate the ratio of the vorticity gap at the front to the total volume transport at the outflow through calculation of the difference in U and its accumulation (integration) from the northern boundary of the grid, as described below. Before that, the parts of K91 relevant to the present study will be briefly introduced.

Under conditions of stratification with a deep and passive lower layer, together with a small Rossby number, $\varepsilon << 1$, and using the governing equations of the upper layer without viscosity and diffusion, K91 set the geostrophic stream function with respect to the second order term, $O(\varepsilon)$, along the north–south section at the outlet of the strait as follows.

$$\psi_{(\alpha)} = \begin{cases} 0 & \text{for } \alpha \le -w \\ \dfrac{h_0 + P\{\cosh l - 1\}}{\sinh w} & \sinh(\alpha + w) \\ h_0 & \text{for } \alpha \ge 0 \end{cases}$$

$$- \begin{cases} 0 & \text{for } -w < \alpha \le -l, \\ P\{\cosh(\alpha + l) - 1\} & \text{for } -l < \alpha \le 0, \end{cases} \quad (1)$$

Here, α denotes the north–south direction (southward positive), $\alpha = 0$ indicates the southern edge of the strait (Figure S1), and w is the width of the strait. In addition, h_0 represents the total volume transport of the outflow, and P represents the gap in vorticity at the front, that is,

with respect to the distribution of the potential vorticity, q, along the section at the outlet, which we defined as (Figure S1):

$$q = \nabla^2\psi - \psi = \begin{cases} -P & \text{for } -l \le \alpha < 0, \\ 0 & \text{for } -w < \alpha < -l, \end{cases} \quad (2)$$

The ratio of the volume transport of the low potential vorticity fluid ($q = -P$, $P > 0$) to the total volume transport Q_R can be written as follows:

$$Q_R = 1 - \psi_{(-l)}/h_0, \quad (3)$$

On the other hand, K91 set the distribution of the stream function in the β (west–east) direction in the downstream region ($\alpha \to \infty$) as follows:

$$\psi_{(\beta)} = \{h_0 + P(\cosh L - 1)\}e^{-\beta} - \begin{cases} P\{\cosh(L-\beta) - 1\} & \text{for } \beta < L, \\ 0 & \text{for } \beta \ge L, \end{cases} \quad (4)$$

where L is the front location from the western boundary (Figure S1). The ratio of the transport of the low potential vorticity fluid to the total transport there, Q_{Rc}, can be written as follows:

$$Q_{Rc} = \begin{cases} 1 - P/2h_0 & \text{for } P/h_0 < 1, \\ h_0/2P & \text{for } P/h_0 \ge 1, \end{cases} \quad (5)$$

Then, following Stern (1986), K91 provided the condition regarding the propagating direction of the long frontal wave using the parameters referred to above:

$$c = \{h_0 - P(1 - e^{-L})\}e^{-L}, \quad (6)$$

where, c is the propagating speed of the long frontal wave. Thus, when c is negative, the wave propagates upstream. Using this condition, K91 defined three domains in the P/h_0–Q_R

plane as a diagnostic diagram for the flow pattern: (I) a steady coastal mode with $Q_R < Q_{Rc}$, (II) a widening coastal mode with $Q_R > Q_{Rc}$ and $P/h_0 < 1$, and (III) a gyre mode with $Q_R > Q_{Rc}$ and $P/h_0 \geq 1$. We applied this diagnostic diagram to the parameters estimated from the surface velocity data obtained from MORSETS.

First, we estimated the ratio of the volume transport of the low potential vorticity fluid to the total volume transport along the outlet of the strait, Q_R. We defined the accumulation of the climatological mean of the zonal velocity from the northern boundary as ψ', assuming that ψ' at the northern boundary was zero. The accumulations at the axis of the jet and the southern coastal boundary or boundary of the HFR observation (Figure 1c) were defined as $\psi'_{(-l)}$ and h_0', respectively. Then, equivalent Q_R' was defined as:

$$Q_R' = 1 - \psi'_{(-l)}/h_0', \quad (7)$$

Here, we assumed that $\psi'_{(-l)}/h_0$' was equivalent to $\psi_{(-l)}/h_0$ as defined by K91.

Second, we estimated the ratio of the gap in the vorticity at the front to the total volume transport, P'/h_0', as follows. The difference in the zonal velocity, $\psi'_{\alpha\alpha}$, was calculated as the representation of the second derivative of the geostrophic stream function. The locations of the maximum and minimum of $\psi'_{\alpha\alpha}$ were defined as α_1 and α_2 (Figure 2c and d). When the multiple maxima were obtained, especially in winter, we defined the location of the northern maximum as α_1 and the adjacent southern minimum as α_2 (Figure 2d), because the southern coastal mode of the TWC in winter has larger Rossby number (>0.4) than that of the northern coastal mode (<0.4; T. Yasui, personal communication, 2021). Then, in the present study, the equivalent gap in the vorticity at the front, P', was estimated using observed gap, $\psi'_{\alpha\alpha(\alpha1)} - \psi'_{\alpha\alpha(\alpha2)}$, as follows:

$$P' = \psi'_{(-l)} \times \left(\psi'_{\alpha\alpha(\alpha_1)} - \psi'_{\alpha\alpha(\alpha_2)}\right)/\psi'_{\alpha\alpha(\alpha_1)}, \quad (8)$$

Assuming that $P'/h_0' = P/h_0$, we used P'/h_0' as another parameter in the diagnosis. Then, the maximum value of the ratio of the volume transport of the low potential vorticity fluid to the total volume transport in the far downstream region, Q_{Rc}', was defined following K91.

Using the parameters Q_R', Q_{Rc}', and P'/h_0', we investigated the flow pattern of TWC based on the diagram suggested by K91. The index of the flow pattern (coastal or gyre) was defined using the intensity of the meridional velocity at the outlet of the strait. The climatological mean of the meridional velocity in each bin (Figure 1c), V (northward positive), was calculated. Then, the meridional average of the velocity over the area 41.51–41.67°N was calculated in each bin located between 141.42°E and 141.63°E for each day as $\langle V \rangle_{41.51-41.67°N}$. Seasonal changes in the meridional velocity at the outlet of the strait are shown in the Results and Figure 3. Then, the zonal mean (141.42–141.63°E for Q_R', Q_{Rc}', and P'/h_0', and 141.54–142.04°E for $\langle V \rangle_{41.51-41.67°N}$) was calculated again to plot the parameters on the Q_R–P/h_0 plane, and we diagnosed the flow pattern by comparing it with the meridional velocity at the outlet (Figure 4).

3 Results

The seasonal distribution of U across the strait at 141.29–141.38°E (Region-a) and at 141.50–141.58°E (Region-b) are shown as examples in Figure 2a and b, respectively. Both figures indicate a northward shift of the eastward jet, and an opposite westward flow to the south of the jet in summer, implying the occurrence of an anticyclonic flow structure south of the jet. In Region-b, U shows a bimodal distribution, with a stronger coastal peak and the other a weaker enhancement in the center of the strait (41.7–41.8°N, Figure 2b). Whereas the intensity of U around the axis increased during summer in Region-a, in Region-b, U near the coast increased

during winter (Figure 2b). In other words, our results suggest the disappearance of the near-coast eastward current at the outlet in summer. This seasonal shift of the jet axis within the strait was consistent with that reported by Abe et al. (2020).

The distribution of $\psi'_{\alpha\alpha}$ also showed a clear seasonal variation (Figure 2c and d) associated with that of U. An increase in the vorticity gap across the front coincident with the axis was recognized in summer. This was especially evident in Region-b, where the spring–summer bimodal distribution was replaced by a well-defined single maximum to the north of the jet axis, and a clear minimum near the southern boundary of the vorticity (Figure 2d).

Consequently, the large gap between the pair was estimated at the outlet of the strait as a result of the enhanced single-peak jet having a spatial scale similar to that of the width of the strait. On the other hand, h_0' calculated as an accumulation of U along the meridional direction, also showed an increase in summer, especially in Region-a (Figure 2c). Thus, as a next step, we calculated the ratio of P' to h_0' for each climatological day from January 1st to December 31st, and compared its spatio-temporal plot with that of Q_R'.

The seasonal variation of P'/h_0' showed clear intensification during the summer, reaching a value of 2.5 (Figure 3a). This seasonal contrast in P'/h_0' was especially remarkable in the region above the Shiriya Spur (141.4–141.6°E, Figure S2). The maximum value of 2.5 occurred in August in this region, and from June to November it was generally greater than 1. In contrast, after November, P'/h_0' decreased rapidly to less than 1. In addition to the high value of P'/h_0' during summer, Q_R' also showed a relatively large value (0.3–0.5) between June and November, although Q_R' temporarily became smaller than 0.3 in August when P'/h_0' reached its maximum. The meridional velocity in the region of the outlet showed the development of northward velocity from June to the middle of August, and this continued until November (Figure 3b). The

peak date of P'/h_0' corresponded with that of the northward velocity (mid-August). Thus, we suggest that the gyre develops from June to mid-August under the high P'/h_0' conditions. The maintenance of the gyre is also implied until November under conditions of $P'/h_0' = 1.0–1.5$ and $Q_R' = 0.3–0.5$, which is consistent with the findings of previous studies (e.g., Conlon, 1982; Rosa et al., 2007). In the upstream region of 141.1–141.4°E, although P'/h_0' generally exceeded 1 throughout year, Q_R' remained below 0.3, except during summer, which implies that the conditions required for gyre development were also established during the summer (Figure 3a).

Next, to compare the result obtained from our HFR observations with the theory suggested by K91, we calculated the zonal mean of P'/h_0' and Q_R' over the region 141.42–141.63°E, at just the outlet of the strait (Figures 3 and S2). After that, each parameter was plotted on the diagnostic diagram proposed by K91 using a color scale to indicate the meridional velocity at the outlet (Figure 4). The result was clearly consistent with K91; i.e., the dots located in the gyre (coastal) mode region showed an intense northward (southward) current at the outlet of the strait. Although an increase in Q_R' to 0.3–0.5, together with a P'/h_0' value of slightly less than 1, were evident in spring (April–June), the current direction around the outlet of the strait was towards the south, suggesting that the gyre does not develop under these conditions. In contrast, although Q_R' showed a constant value of approximately 0.3 during the summer (July–September), the northward current around the outlet was indicated by the large value of P'/h_0' (>1.5).

4 Discussion

Our results are consistent with the theory proposed by K91 (Figure 4). Therefore, the importance of the vorticity gap at the front (the axis of the TWC) as a factor in gyre formation (in addition to the volume transport of the TWC) has been confirmed again using our observational data obtained from the HFR. With respect to the annual data, the distribution of each parameter in the diagnostic diagram was similar to that of the six-year climatological data, although there were exceptions. Consequently, we conclude that our results support the reliability and effectiveness of using high-resolution HFR observations with the diagnostic scheme, and also its applicability to other coastal regions such as the Alboran Sea. However, note that the TWC shows large seasonal variability in stratification (e.g., Sugimoto and Kawasaki, 1984), and this kind of diagnostic approach should be treated with caution, especially in winter when the stratification is weaker.

To test our HFR approach, we also applied it to an upstream region of the same strait (Figure S3). One of the notable characteristics of the seasonal changes in the flow within the upper section of the strait during summer was the disappearance of the coastal eastward current at the outlet and the northward shift of the flow, which had only a single axis (Figure 2b). This caused the sharp single peak in the jet and the large vorticity gap at the front, which contributed to the mode change. The cause of the disappearance and shift in the flow remains one of the issues to be addressed. The application of the theory of outflow from the strait may be reasonable, because the coastline of the peninsula extends southwards in the region east of 141.1 °E (Figure S3a). Thus, frontal wave stagnation there may occur as another sub-gyre in the region. In fact, in summer, negative vorticity development related to the meridional velocity was evident around 141.2–141.4°E (Figure S3b) in association with the high P/h_0 conditions in the

region 141–141.2°E (Figure S3c). Development of the sub-gyre could push the axis to the north, and weaken the downstream flow along the northern coast. Note that this approach in this upstream region should be treated with caution, again, because the Rossby number in this region would be larger than that in the outlet of the strait. Thus, investigations of the sub-gyre development are ongoing based on the coastal monitoring networks of MORSETS. Moreover, the cause of seasonal change in the jet form should also be examined in relation to other physical processes, including water mass distribution, tides, and volume transport by the TWC itself (which would be related to wind stress curl).

The modulation of TWC such as the developments of the gyres during summer, suggests that the Tsugaru Strait has an important impact on the system of the currents along the Japanese coast including the Tsushima Warm Current, and the Kuroshio. Kida et al. (2020) explained that the increasing trend seen in the volume transport of the Tsushima Warm Current reflects the long-term northward (coastward) shift of the Kuroshio axis. This interpretation was based on the assumption that the integration of the horizontal frictional torque caused by the coastal flow around the islands (including Honshu, Kyushu, and Shikoku; Figure 1a) should be zero under steady-state conditions (Yang, 2007; Kida et al., 2016). The development of the gyre and the associated offshore movement of the flow path in the Tsugaru Strait may affect the integration of the horizontal frictional torque caused by the coastal flow. Thus, it will be worthwhile investigating the role of the Tsugaru Strait more carefully in relation to the increasing trend in the volume transport in the upstream region.

Moreover, the decadal variability of the circulation within the upstream region may cause similar variations in the TWC. Kaneko et al. (2018) reported a shift in the Kuroshio axis along 141°N, which was synchronous with both a stable Kuroshio Extension and the Pacific Decadal

Oscillation, and this situation persisted for about 10 years after the 1998/1999 regime shift. If such a synchronized shift of the axis could cause changes in the transport of the TWC, rapid changes in biota synchronized with the shift might be caused along the warm currents around Japan, including the TWC. Recently, the northward expansion of harmful dinoflagellates into the strait, which can cause red tides, was reported, and transport by the TWC was suspected as one of causes (Shimada et al., 2016). Therefore, in future, the role of the eastern part of the Tsugaru Strait in the modulation of the flows should be clarified with respect to both long-term trends and decadal variations, as this could have a large impact on the biota. Enlargement of HFR observations, development of high-resolution numerical models, and enhancing the coastal observation networks, including monitoring buoys, would all contribute to this task.

Acknowledgments

The The authors acknowledge the help of the staff of the Mutsu Institute for Oceanography and the Research Institute for Global Change of JAMSTEC. The HFR data used in the present study was distributed through MIO, JAMSTEC (https://www.godac.jamstec.go.jp/morsets/e/top/). We sincerely acknowledge the technical support staff from Marine Work Japan. We also thank Dr. M. Wakita, T. Yasui, S. Tatamisashi, T. Hashimukai, T. Nakayama, and S. In for their helpful comments.

References

Abe, H., K. Sasaki, T. Yasui, and M. Wakita (2020) Observation of Tsugaru warm current by High Frequency Radar and preliminary result for its prediction, *Kaiyo Monthly*, 52, 312–316. (in Japanese)

Conlon, D. M. (1982), On the outflow modes of the Tsugaru Warm Current, *La mer*, 20, 60–64.

Isobe, A. (1999) On the origin of the Tsushima Warm Current and its seasonality. *Cont. Shelf Res.*, 19 (1), 117–133. https://doi.org/10.1016/S0278-4343(98)00065-X

Isoda, Y., and K. Baba (1998), Tides and tidal currents in the Tsugaru strait. *Bull. Fac. Fish. Hokkaido Univ.*, 49 (3), 117– 130 (in Japanese with English abstract)

Japan Agency for Marine-Earth Science and Technology MORSETS website (2020), MIO ocean radar data site for Eastern Tsugaru Strait. https://www.godac.jamstec.go.jp/morsets/e/top/. Accessed on 22 Nov. 2020

Kaneko, T. Okunishi, T. Seto, H. Kuroda, S. Itoh, S. Kouketsu, and D. Hasegawa (2018), Dual effects of reversed winter–spring temperatures on year-to-year variation in the recruitment of chub mackerel (*Scomber japonicus*), *Fish. Oceanogr.*, 28, 1–16, https://doi.org/10.1111/fog.12403

Kawasaki, Y. and T. Sugimoto (1988), A laboratory study of the short-term variation of the outflow pattern of the Tsugaru Warm Water with a change in its volume transport. *Bull. Tohoku Reg. Fish. Res. Lab.*, 50, 203–215 (in Japanese with English abstract)

Kida, S., B. Qi, J. Yang, and X. Lin (2016) The annual cycle of the Japan Sea Throughflow. *J. Phys. Oceanogr.*, 46 (1), 23–39, doi: 10.1175/JPO-D-15-0075.1

Kida, S., K. Takayama, Y. N. Sasaki, H. Matsuura, and N. Hirose (2020), Increasing trend in Japan Sea Throughflow transport, *J. Oceanogr.*, https://doi.org/10.1007/s10872-020-00563-5

Kubokawa, A. (1991), On the behavior of outflows with low potential vorticity from a sea strait. *Tellus A*, 43, 168–176. https://doi.org/10.1034/j.1600-0870.1991.t01-1-00007.x

Luu, Q. H., K. Ito, Y. Ishikawa, and T. Awaji (2011), Tidal transport through the Tsugaru Strait — part I: Characteristics of the major tidal flow and its residual current. *Ocean Sci. J.*, 46, 273–288. https://doi.org/10.1007/s12601-011-0021-z

Matsuura, H., and Y. Isoda (2020), Pseudo-fortnightly variation produced by interaction between passage-flow and diurnal tidal currents in the Tsugaru Strait, *Bull. Fac. Fish. Hokkaido Univ.*, 70 (1), 13–23, doi:10.14943/bull.fish.70.1.13

Nishida, Y., I. Kanomata, I. Tanaka, S. Sato, S. Takahashi, and H. Matsubara (2003), Seasonal and Interannual Variations of the Volume transport through the Tsugaru Strait. *Oceanogr. Jpn*, 12 (5), 487–499, https://doi.org/10.5928/kaiyou.12.487 (in Japanese with English abstract)

Nof, D., and T. Pichevin (1999) The Establishment of the Tsugaru and the Alboran Gyres. *J. Phis. Oceanogr.*, 29(1), 39–54, DOI: https://doi.org/10.1175/1520-0485(1999)029<0039:TEOTTA>2.0.CO;2

Onishi, M., and K. Ohtani (1997) Volume transport of the Tsushima Warm Current, west of Tsugaru Strait bifurcation area. *J. Oceanogr.*, 53(1), 27–34,

Onishi M., Y. Isoda, H. Kuroda, M. Iwahashi, C. Saitoh, T. Nakayama, T. Ito, K. Iseda, K. Nishizawa, S. Shima, and O. Togawa (2004), Winter Transport and Tidal Current in the Tsugaru Strait. *Bull. Fac. Fish. Hokkaido Univ.*, 55 (2), 105–119.

Ohta, S., Y. Isoda, S. Yoshimura, K, Syouji, S. Arita, K. Kawano, X. Fang, and N. Kobayashi (2014), Internal tidal waves generated over the sill topography in the Tsugaru Strait, *Sea and Sky*, 90 (5), 63–84, (in Japanese with English abstract)

Rosa, A. L., Y. Isoda, K. Uehara, and T. Aiki (2007), Seasonal Variations of Water System Distribution and Flow Patterns in the Southern Sea Area of Hokkaido, Japan. *J. Oceanogr.*, 63, 573–588, doi:10.1007/s10872-007-0051-4.

Shimada, H., M. Kanamori, H. Yoshida, and I. Imai (2016), First record of red tide due to the harmful dinoflagellate *Karenia mikimotoi* in Hakodate Bay, southern Hokkaido, in autumn, 2015. *Nippon Suisan Gakk.*, 82(6), 934–938, https://doi.org/10.2331/suisan.16-00033, (in Japanese with English abstract)

Stern, M. E. (1986), On the amplification of convergences in coastal currents and the formation of "squirts". *J. Mar. Res.*, 44 (3), 403–421, https://doi.org/10.1357/002224086788403097

Sugimoto, T., and Y. Kawasakai (1984) Seasonal and year-to- year variations of the Tsugaru Warm Current and their dynamical interpretation. *Bull. Coastal Oceanogr*., 22, 1–11 (in Japanese).

Tanaka, T, H. Hasegawa, T. Okunishi, H. Kaneko, and T. Ono (2021), Internal Hydraulic Jump in the Tsugaru Strait, *J. Oceanogr.* https://doi.org/10.1007/s10872-020-00588-w

Yamaguchi, T., Y. Isoda, U. Itoh, T. Mukai, and N. Kobayashi (2020), Observation and model experiments on an internal-wave packet accompanied by streak bands over the sill topography of Tsugaru Strait, *Oceanogr. Jpn,* 29 (3), 71–90, https://doi.org/10.5928/kaiyou.29.3_71 (in Japanese with English abstract)

Yang, J. (2007), An oceanic current against the wind: how does Taiwan Island steer warm water into the East China Sea? *J. Phys. Oceanogr.*, 37 (10) 2563–2569, doi: 10.1175/JPO3134.1

Yoshikawa, Y., A. Masuda, K. Marubayashi, M. Ishibashi, and A. Okuno (2006), On the accuracy of HF radar measurement in the Tsushima Strait, *J. Geophys. Res.*, 111, C04009, doi:10.1029/2005JC003232.

Figure captions

Figure 1. (a) Schematic diagram of the flows around Japan. (b) Seasonal flow pattern of the Tsugaru Warm Current. (c) Observation site of the present study and distribution of the temporal mean velocity at each grid point. The square grids in (c) indicate the bins used to calculate the zonal average of the zonal velocity.

Figure 2. Examples of date–latitude plots of (a) and (b) zonal velocity, and (c) and (d) ψ' (thin lines) and $\psi'_{\alpha\alpha}$ (color and thick lines). The left (right) column denotes Region-a (Region-b). The black line in (a) and (b) denotes the latitude of the jet axis. The orange (blue) line in (c) and (d) denotes the latitude of the maximum (minimum) of $\psi'_{\alpha\alpha}$. See text for definitions of ψ' and $\psi'_{\alpha\alpha}$.

Figure 3. Longitude–date plot of (a) Q_R' (color) and P'/h_0' (contours), and (b) meridional velocity averaged in north–south band. See text for definitions of Q_R', P', and h_0'.

Figure 4. The diagnostic diagram for the flow pattern.

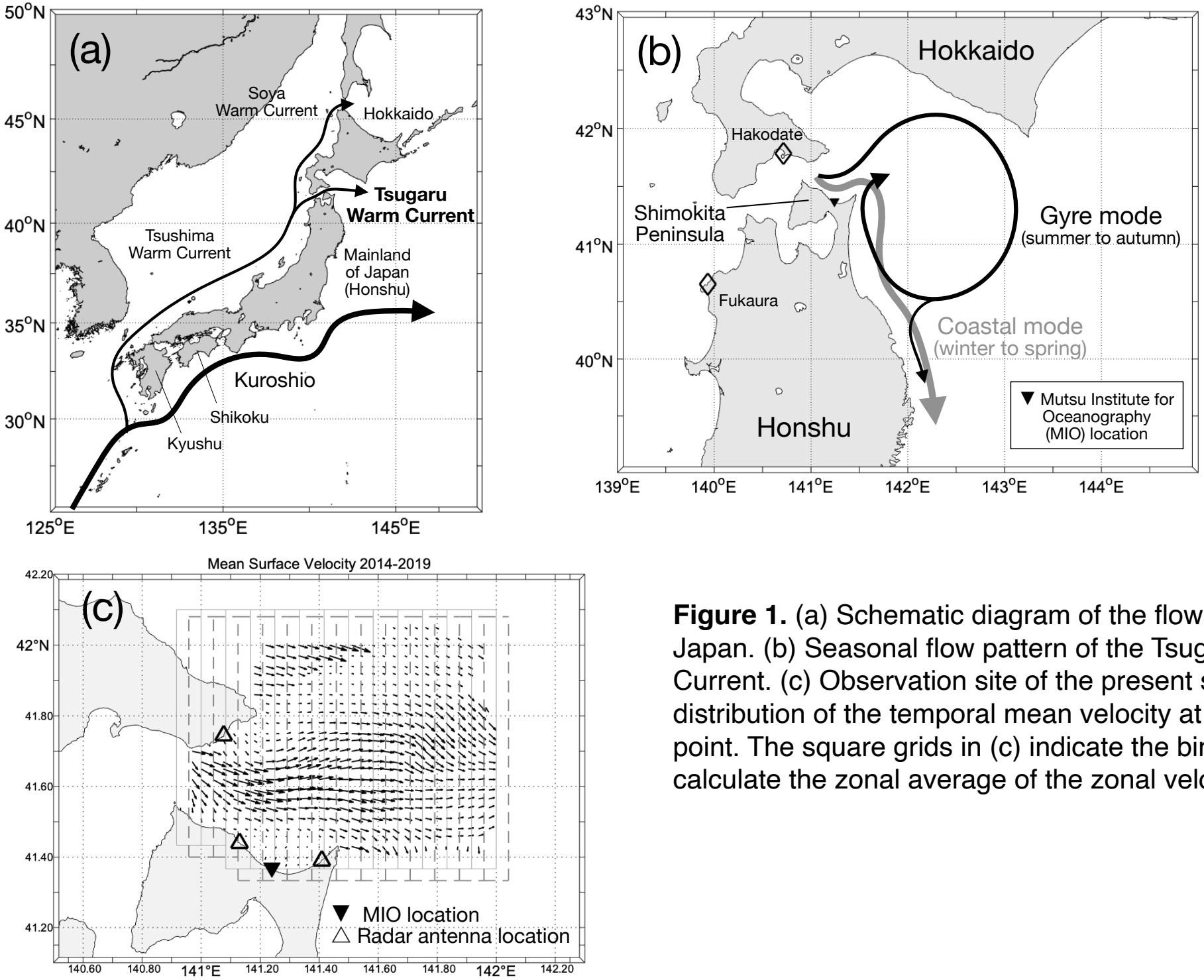

Figure 1. (a) Schematic diagram of the flows around Japan. (b) Seasonal flow pattern of the Tsugaru Warm Current. (c) Observation site of the present study and distribution of the temporal mean velocity at each grid point. The square grids in (c) indicate the bins used to calculate the zonal average of the zonal velocity.

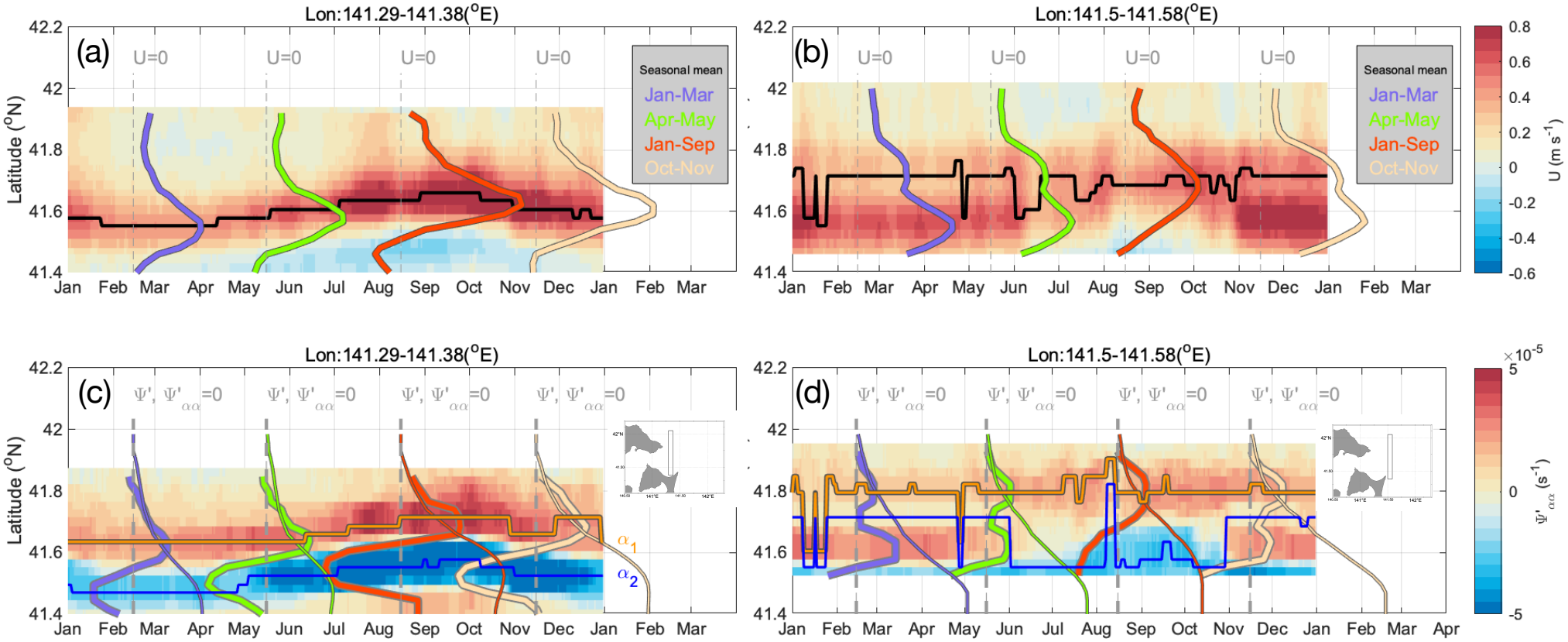

Figure 2. Examples of date–latitude plots of (a) and (b) zonal velocity, and (c) and (d) ψ' (thin lines) and $\psi_{\alpha\alpha}$' (color and thick lines). The left (right) column denotes Region-a (Region-b). The black line in (a) and (b) denotes the latitude of the jet axis. The orange (blue) line in (c) and (d) denotes the latitude of the maximum (minimum) of $\psi_{\alpha\alpha}$'. See text for definitions of ψ' and $\psi_{\alpha\alpha}$'.

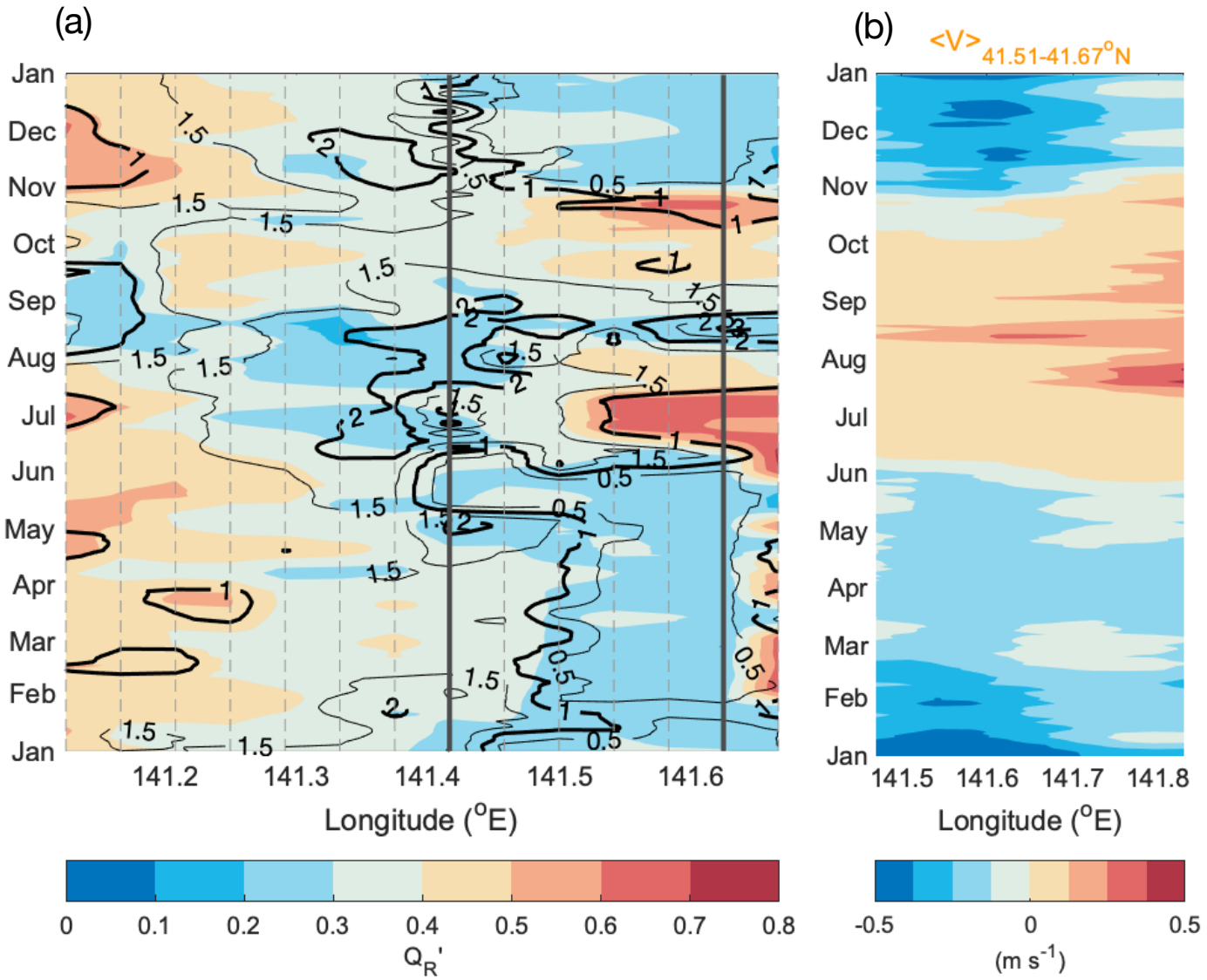

Figure 3. Longitude–date plot of (a) Q_R' (color) and P'/h0' (contours), and (b) meridional velocity averaged in north–south band. See text for definitions of Q_R', P', and h_0'.

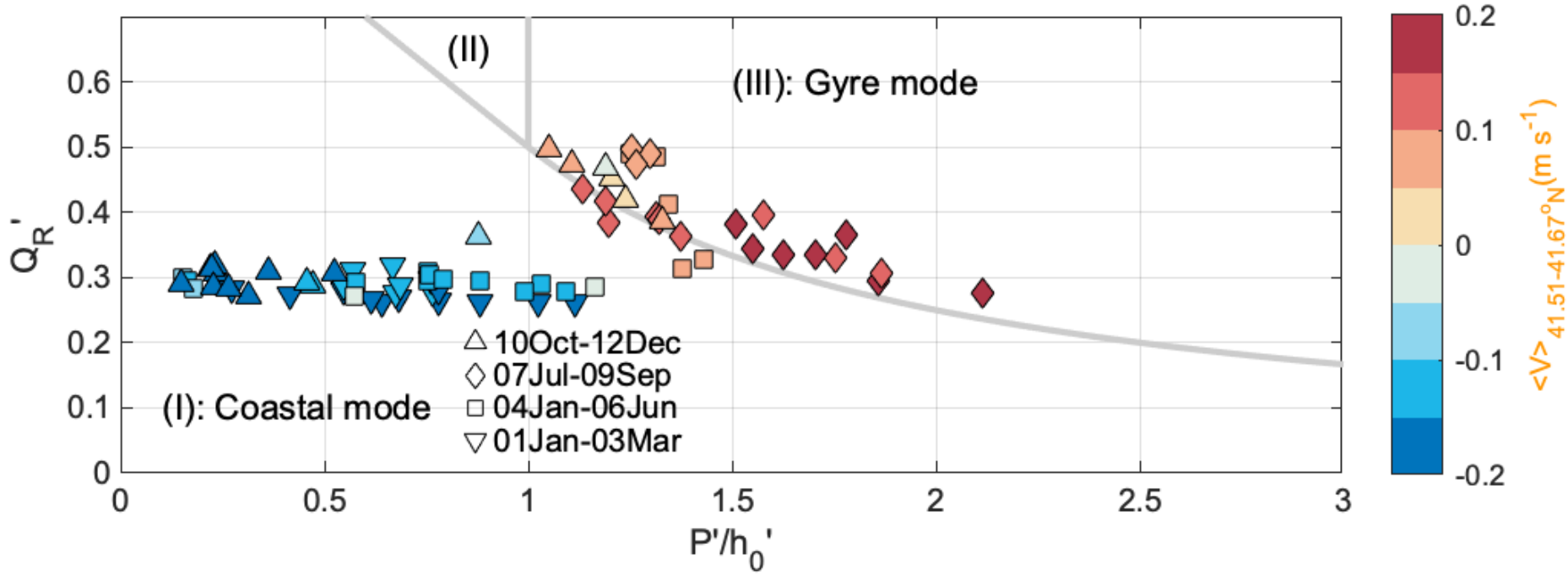

Figure 4. A diagnosis diagram of the flow pattern.